Improved power simulation of AlGaN/GaN HEMT at class-AB operation via an RF drain–source current correction method*

Pongthavornkamol Tiwat(林体元)†, Pang Lei(庞 磊), Yuan Ting-Ting(袁婷婷), and Liu Xin-Yu(刘新宇)

Key Laboratory of Microelectronics Devices & Integrated Technology, Institute of Microelectronics, Chinese Academy of Sciences, Beijing 100029, *China*

(Received 19 June 2014; revised manuscript received 24 July 2014; published online 10 October 2014)

A new modified Angelov current–voltage characteristic model equation is proposed to improve the drain–source current (I_{ds}) simulation of an AlGaN/GaN-based (gallium nitride) high electron mobility transistor (AlGaN/GaN-based HEMT) at high power operation. Since an accurate radio frequency (RF) current simulation is critical for a correct power simulation of the device, in this paper we propose a method of AlGaN/GaN high electron mobility transistor (HEMT) nonlinear large-signal model extraction with a supplemental modeling of RF drain–source current as a function of RF input power. The improved results of simulated output power, gain, and power added efficiency (PAE) at class-AB quiescent bias of $V_{gs} = -3.5$ V, $V_{ds} = 30$ V with a frequency of 9.6 GHz are presented.

Keywords: AlGaN/GaN HEMT, RF drain–source current, RF dispersion effect, power-added efficiency

PACS: 73.61.Ey, 85.30.De, 85.40.Bh, 84.40.–x **DOI:** 10.1088/1674-1056/23/12/127304

1. Introduction

Radio frequency (RF)-microwave power device research plays an important role in a better power amplifier circuit for high frequency applications such as mobile base station transceivers and satellite communication transmitters. A gallium nitride (GaN)-based high electron mobility transistor (HEMT) is a good option due to its excellent properties such as high output power density,[1] high breakdown voltage,[2] and high thermal performance.[3] Although GaN HEMT is a promising device for RF-microwave power amplifier circuit design, its non-perfect property of nonlinearity at high efficiency mode (e.g. class-AB) still exists. Since a class-AB power amplifier has many advantages such as high efficiency and simplicity of design, it can fulfill the requirements of many communication applications.[4–6]

A disadvantage of the class-AB power amplifier is a generation of nonlinear output signal due to its operating quiescent bias. At this nonlinear quiescent point, drain–source current increases significantly when a higher RF input power is added.[7] Hence, the accurate modeling of a drain–source current of a transistor device in high power operation is needed for accurately predicting the output power, gain, and efficiency of a high power amplifier circuit. In this paper, we propose the improved simulations of drain–source current, output power, gain, and power-added efficiency (PAE) of the device model by modifying parameter 'I_{pk}', which represents the drain–source current for maximum transconductance value in an Angelov current–voltage characteristic equation.[8] In some previous literature the parameter 'I_{pk}' was also modified as a function of quiescent bias and temperature, but for the main purpose of modeling the thermal dependent effect in a GaN HEMT device.[9,10] The proposed method in this paper is to modify I_{pk} as a function of RF input power in order to improve the accuracy of the device's power simulation.

2. AlGaN/GaN HEMT structure

The AlGaN/GaN HEMT device used in this paper is fabricated with silicon carbide as a substrate. The process of metal–organic chemical vapor deposition (CVD) is used in order to grow an AIN spacer layer, an AlGaN barrier layer, and a GaN layer on the substrate. Ohmic contacts are created by depositing Ti/Al/Ni/Au metals followed by rapid thermal annealing at a high temperature (870 °C) in nitrogen gas. A passivation layer of silicon nitride with a thickness of 200 nm is deposited by using a plasma-enhanced CVD system. There are 8 and 10 gate fingers in total. Each finger has a gate width of 100 μm and a gate length of 0.25 μm.

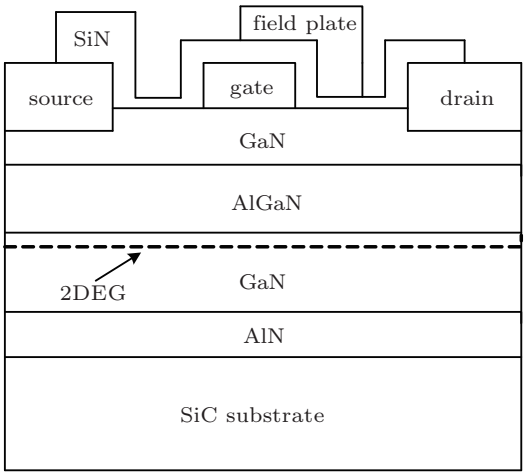


Fig. 1. Cross-sectional structure of AlGaN/GaN HEMT.

*Project supported by the National Natural Science Foundation of China (Grant No. 61204086).

†Corresponding author. E-mail: lintiyuan@ime.ac.cn

© 2014 Chinese Physical Society and IOP Publishing Ltd

Figure 1 shows stacked layers of AlGaN/GaN HEMT in a cross-sectional view. A gate-connected field plate is added for improving the power gain at RF-microwave operating frequencies. The top-view photographs of AlGaN/GaN HEMT devices with gate sizes of 10×100 μm and 8×100 μm are shown in Figs. 2(a) and 2(b) respectively.

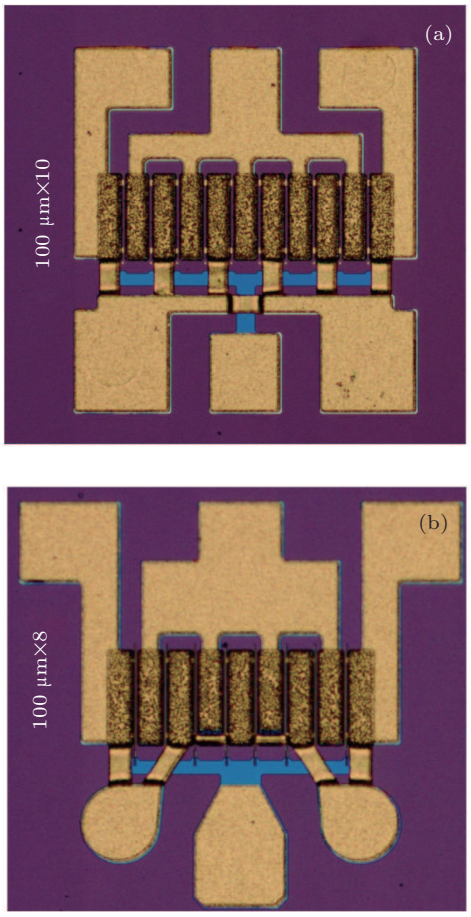


Fig. 2. (color online) AlGaN/GaN HEMT devices with the gate sizes of (a) 10×100 μm and (b) 8×100 μm.

3. DC current modeling

The drain–source currents at various bias points are measured by using a continuous stationary measurement system. The gate–source voltage varies from −5 to −2 V whereas the drain–source voltage varies from 0 V to 30 V. Since the stationary measurement causes the trapping effect at the buffer and surface layers of the HEMT device, the kink effect at low V_{gs} regions can occur.[11] A comparison of I_{ds} between the simulation and measurement is shown in Fig. 3.

The Angelov I–V equations[8] are used to model the measured I_{ds}, and they are shown below

$$I_{ds} = I_{pk}(1+\tanh(\Psi))\cdot\tanh(\alpha V_{ds})\cdot(1+\lambda V_{ds}), \quad (1)$$

$$\Psi = P_1(A\cdot V_{gs}+B-V_{pk})+P_2(A\cdot V_{gs}+B-V_{pk})^2 + \cdots P_n(A\cdot V_{gs}+B-V_{pk})^n, \quad (2)$$

$$V_{pk} = V_{pk0}+\gamma\cdot V_{ds}, \quad (3)$$

where I_{pk} is the drain–source current for the maximum transconductance value, Ψ is the power series function centered at V_{pk}, V_{pk} is the gate voltage for maximum transconductance value, α is the saturation parameter, λ is the channel length modulation parameter, P_n is the coefficients defining the transconductance value at V_{pk}.

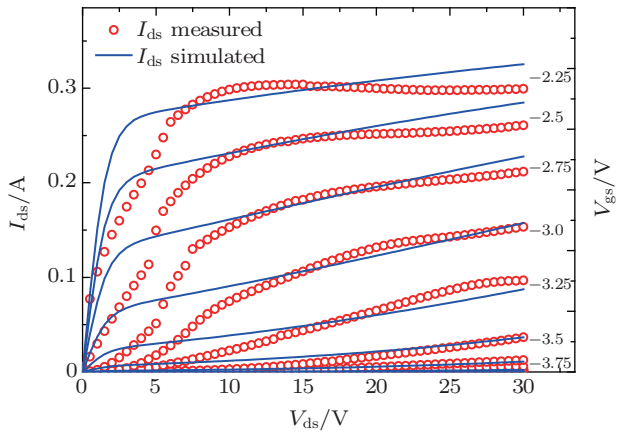


Fig. 3. (color online) Simulated (solid line) and measured (empty circle) current–voltage characteristic curves of I_{ds} for a device with a 10×100 μm gate size.

The three additional coefficients ('A' and 'B' in power series Eq. (2) and 'γ' in Eq. (3)) are obtained from the work of I–V model improvement.[12] The extracted values of parameters in Eqs. (1)–(3) are shown in Table 1.

Table 1. Extracted values of Angelov current–voltage model parameters for a device with a gate size of 10×100 μm.

I_{pk}/mA	λ	α	P_1	P_2	P_3
369	1×10^{-6}	0.65	0.1	1.412×10^{-4}	0.015
P_4	V_{pk0}/V	γ	A	B	
1×10^{-5}	–0.073	–0.0296	2.493	3.622	

The gate–source current (I_{gs}) is also measured during the stationary measurement of I_{ds}. The fitting function of the measured I_{gs} is optimized by a curve fitting tool in MATLAB.

4. Large-signal modeling

In this section, the method of empirical nonlinear model extraction is proposed and followed by the multi-bias capacitance (C_{gs}, C_{gd}, and C_{ds}) models. The validation of the device model for S-parameter simulation in a frequency range of 500 MHz–40 GHz is also presented.

4.1. Equivalent circuit model

The schematic diagram of the AlGaN/GaN HEMT equivalent circuit model is shown in Fig. 4. The simulation of circuit schematics is implemented using advanced design system

(ADS) software. The equations of DC-currents in the previous section are included in the model by using a multi-port component called a 'symbolically defined device' or 'SDD'.

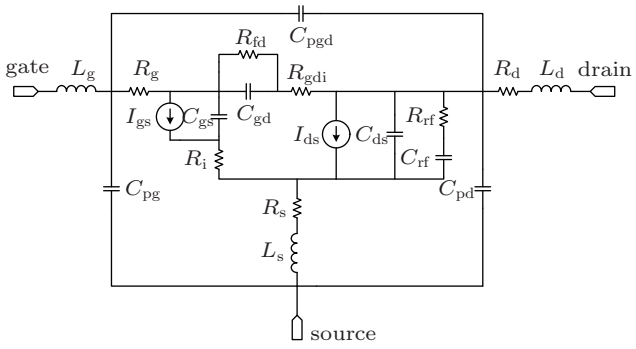


Fig. 4. AlGaN/GaN HEMT equivalent nonlinear circuit model.

The values of the extrinsic parameters (L_g, L_d, L_s, R_g, R_d, R_s, C_{pg}, C_{pd}, C_{pgd}) and intrinsic parameters (R_{rf}, C_{rf}, R_{gdi}, R_i) are optimized and tuned from the starting values, which are calculated via the measurements of reverse biased cold-FET (field-effect transitors) ($V_{ds} < 0$ V) and forward biased hot-FET ($V_{ds} > 0$ V) S-parameters.[13] The optimized values of extrinsic and intrinsic parameters, except three multi-biases-dependent capacitances (C_{gs}, C_{gd}, and C_{ds}), are shown in Table 2.

Table 2. Optimized extrinsic and intrinsic parameters of the device with a gate size of 10×100 μm.

L_g/pH	L_d/pH	L_s/pH	R_g/Ω	R_d/Ω	R_s/Ω	R_{gdi}/Ω
85	35	5	1	2	0.5	1
C_{pg}/pF	C_{pgd}/fF	C_{pd}/fF	R_{rf}/Ω	C_{rf}/pF	R_{fd}/kΩ	R_i/Ω
0.6	10	5	360	1.3	8	5

4.2. Capacitance models

Since the hyperbolic tangential functions presented by Angelov[14] cannot be fitted well to the optimized capacitance values, the 4th-degree polynomial equations of variable biases V_{gs} and V_{ds} are chosen to represent the multi-biase-dependent C_{gs}, C_{gd}, and C_{ds} capacitance models. The optimized coefficients of the capacitance model are obtained from the optimization of the curve fitting tool in MATLAB. The results of curve fitting between polynomial equations and optimized values of C_{gs}, C_{gd}, and C_{ds} are shown in Fig. 5.

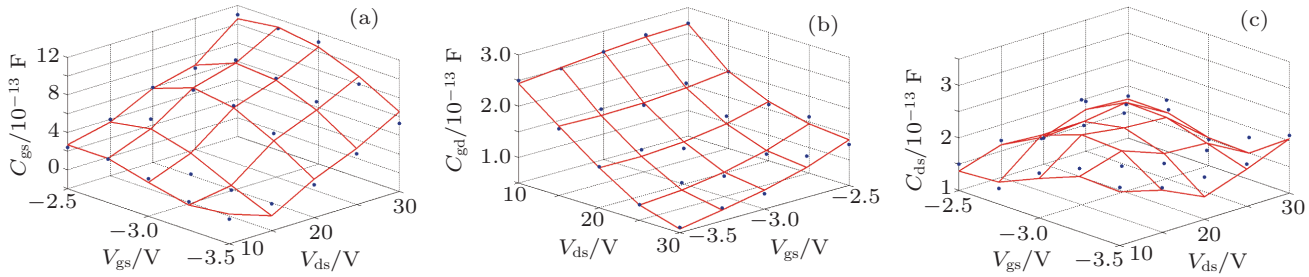


Fig. 5. (color online) Comparison between the polynomial equation curve (mesh) and optimized values (solid circle) at various biased voltages of three capacitance parameters by using polynomial functions in MATLAB curve fitting toolbox: (a) C_{gs}; (b) C_{gd}; and (c) C_{ds}.

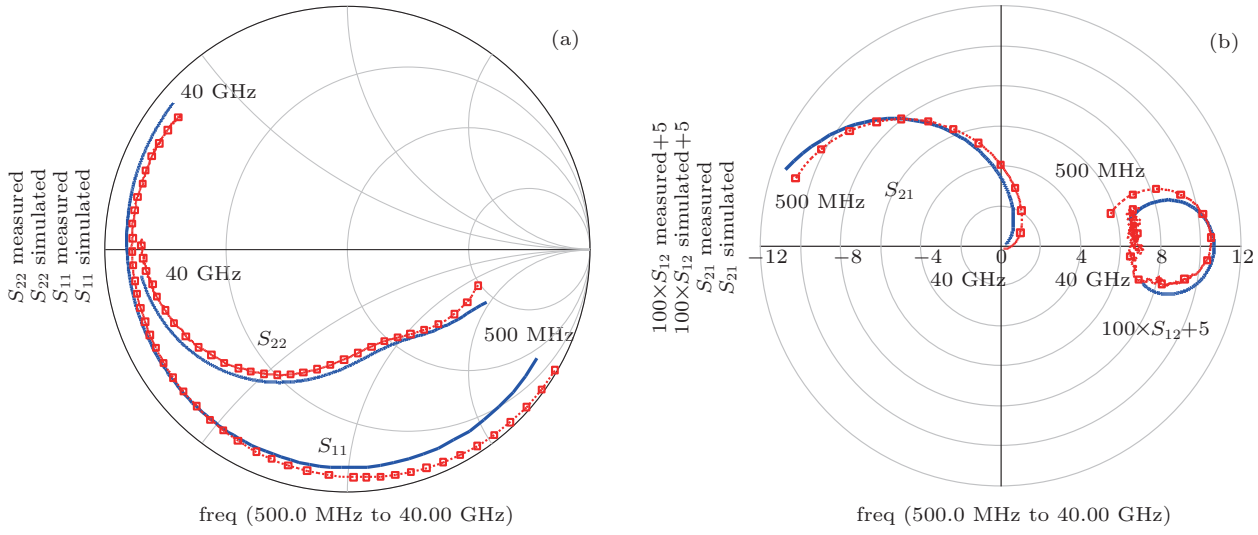


Fig. 6. (color online) Comparisons of S-parameter between measurement (squared line) and simulation (solid line) in a frequency range of 500 MHz–40 GHz for a device with a gate size of 10×100 μm, $V_{gs} = -3.5$ V, and $V_{ds} = 30$ V, where panel (a) shows S_{11} and S_{22}, and panel (b) display S_{21} and S_{12}.

4.3. *S*-parameter validation

The two-port *S*-parameters are measured by an Agilent 8510C network analyzer and on-wafer probe measurement system in a frequency range of 500 MHz–40 GHz. The calibration method is the Short-Open-Load-Through method. The measurements are performed with a 50-Ω characteristic impedance system. For the verification of the model, the stationary measurements of *S*-parameters are compared with the simulations of the model from ADS at class-AB operating point ($V_{gs} = -3.5$ V, $V_{ds} = 30$ V). The comparison between simulation results in a frequency range of 500 MHz–40 GHz are shown in the Smith charts (S_{11}, S_{22}) and Polar charts (S_{21}, S_{12}) of Fig. 6.

5. RF power simulation

Other important properties of the device model for power amplifier design are output power, gain, and PAE. In order to reach the maximum value of measured output power, the RF load-pull system is used to search the optimum input- and output-impedances of the device. This technique is also an essential step for designing a high power amplifier. In order to avoid a self-heating effect of the device during the power measurement, the load-pull measurement is performed by a pulse operation of 10%-duty cycle with 100-μs pulse period. The RF power simulation is implemented by using a harmonic balance simulation tool in ADS software. The operating frequency is 9.6 GHz at class-AB biased voltage point ($V_{gs} = -3.5$ V, $V_{ds} = 30$ V). From the automatic tuning result of the RF load-pull system, the optimum input impedance result at this operating frequency is $5.58 + \mathrm{j}5.91$ Ω whereas the optimum output impedance is $20.74 + \mathrm{j}30.12$ Ω. The input power (P_{in}) is swept from −10 dBm to 10 dBm and from 20 dBm to 28 dBm. The dynamic loadlines of the power simulation at different input power levels are shown in Fig. 7.

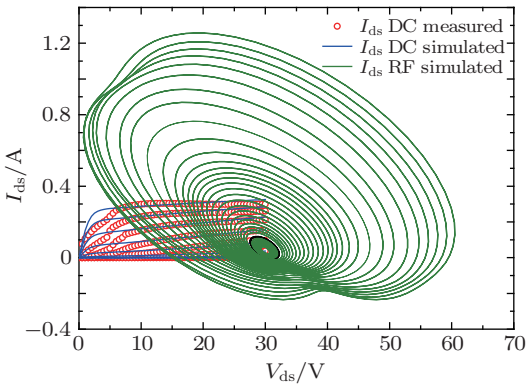


Fig. 7. (color online) Dynamic loadline simulations of AlGaN/GaN HEMT with input power sweeping at class-AB operation point ($V_{gs} = -3.5$ V, $V_{ds} = 30$ V) with an operating frequency of 9.6 GHz for a device with a gate size of 10×100 μm ($P_{in} = 0$ dBm–28 dBm in steps of 1 dBm).

From the simulated loadlines, it can be observed that if the quiescent biased drain–source voltage (V_{ds}) is high enough, the kink effect at low V_{ds} does not affect the power simulation even in the case of a high input power. Furthermore, it can be noticed that the loadlines at a high input power show an irregular shape of eclipse because their quiescent biased voltage points are at nonlinear class-AB operation. The nonlinear waveform at class-AB operation ($V_{gs} = -3.5$ V, $V_{ds} = 30$ V) can be seen in the time-domain simulation of I_{ds} in Fig. 8. It can be seen that the average value of I_{ds} waveform increases when the RF input power is higher.

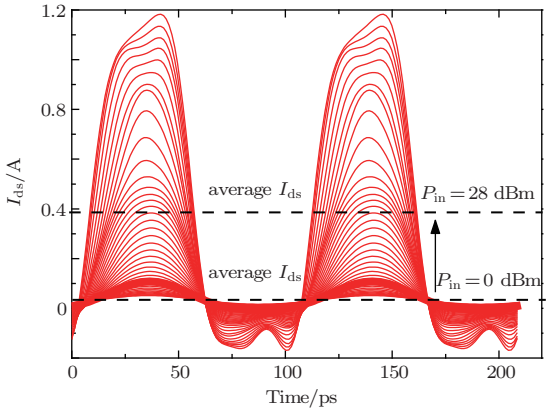


Fig. 8. (color online) Time-domain waveform simulations of drain–source current with different input powers at an operating frequency of 9.6 GHz for a device with a gate size of 10×100 μm ($P_{in} = 0$ dBm–28 dBm in steps of 1 dBm).

The nonlinearity of the HEMT device at class-AB operation can result in the shifting up of the quiescent point while the input power keeps increasing. This is because, when the input power is increased, the magnitudes of waveform amplitudes in both positive and negative regions are enlarged as shown in Fig. 8. Since the increment of the amplitude in the negative pinch-off region is small when compared with the positive region, the value in the negative region does not affect the calculation of the average value of I_{ds} very much. This phenomenon leads to the continuous increase of the measured drain–source current of the device when the operating bias is located at class-AB point. Even though the designers have to deal with this kind of nonlinear problem, the class-AB operating biased points can still be selected for the power amplifier circuit design due to its advantage of high efficiency. Hence, the increase of I_{ds} must be modeled correctly because the precision of drain–source current simulation is an important factor in accurate power simulation.

5.1. RF drain–source current modeling

Modeling the RF drain–source current, we find that one of the problems is an underestimation of simulated drain–source current (I_{ds}) at the high input power points. The simulation of drain–source current is lower than the measurement. This discrepancy between DC- and RF-drain currents is known as the RF dispersion effect in the AlGaN/GaN HEMT device. The RF dispersion effect causes the transconductance to be inconsistent when the operation is changed from DC to RF.[15] Since

the Angelov's drain–source current equations (1)–(3) contain only the description of DC operation, an additional modification of drain–source current should be added to these equations in order to obtain the better simulation of drain–source current at RF operation. The new solution is to modify the parameter 'I_{pk}' of I_{ds} in Eq. (1). This is because the dispersion effect increases the RF drain–source current at various bias points, including the bias point at a maximum value of transconductance. Hence, the parameter that represents the drain–source current value at the maximum transconductance (i.e. 'I_{pk}') should be increased when the dispersion effect becomes more dominant at high RF input power. This means that the I_{pk} parameter can be modeled as a function of variable RF input power. The new modification of 'I_{pk}' at high RF input power can be written as the following equations:

for $P_{in} < P_{in,3\ dB}$,

$$I_{pk,modified}(P_{in}) = I_{pk,DC} + I_{pk,RF} = I_{pk,DC} + (P_{in} - P_0)\cdot\beta, \quad (4)$$

for $P_{in} \geq P_{in,3\ dB}$,

$$I_{pk,modified}(P_{in}) = \text{const.} = I_{pk,DC} + (P_{in,3\ dB} - P_0)\cdot\beta, \quad (5)$$

where $I_{pk,DC}$ is the drain–source current for maximum transconductance value at DC operation, $I_{pk,RF}$ is the additional drain–source current for maximum transconductance value at RF operation, P_0 is the maximum input power in dBm at which the drain–source current simulation is still accurate, P_{in} is the input power in dBm, higher than P_0, $P_{in,3\ dB}$ is the input power in dBm at 3-dB compressed gain point, and β is the fitting slope parameter.

The modified equation (4) is applicable only when the input power is swept beyond the maximum input power that still contains good correlation between simulated and measured drain–source current (i.e. "P_0"). In this paper, 'P_0' is equal to 22 dBm. The value of parameter '$I_{pk,DC}$' in Eqs. (4) and (5) is equal to the value of I_{pk} in Table 1. The drain–source current in the RF operation is calculated from the product, i.e. the difference between two input power points (P_{in}–P_0) multiplied by the fitting slope parameter (β) for optimum simulated output power and gain. In this paper, we set the fitting slope parameter $\beta = 0.02$. Since the quiescent drain–source current is saturated at the input power of $P_{in,3\ dB} = 27$ dBm (3-dB compressed gain point), the value of $I_{pk,RF}$ at such a gain point or higher is also saturated at a constant value of $(P_{in,3\ dB}–P_0)\cdot\beta$ as shown in Eq. (5).

After the modification of I_{pk}, the comparison between RF drain–source current simulation with 24-dBm RF input power and DC drain–source current measurement can be plotted in Fig. 9. This comparison can reflect the RF dispersion effect of the AlGaN/GaN HEMT device. The simulated result of $I_{ds,RF}$ is also consistent with the result in the textbook by Gao[16] which shows that the RF drain–source current simulation can be constructed by extracting the transconductance (g_m) and output conductance (g_{ds}) from the S-parameters measurement.

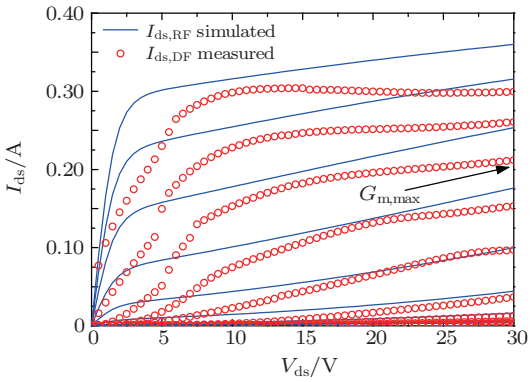


Fig. 9. (color online) Comparison between RF drain–source current simulation and DC drain–source current measurement after the modification of I_{pk} parameter ($V_{gs} = -5$ V to -2.25 V in steps of 0.25 V) for a device with a gate size of 10×100 μm.

5.2. Improved simulations

Using the modified Angelov I–V equation, the accuracy of simulated I_{ds} current at high input power can be improved, as shown in Fig. 10. The improvements in output power and gain about 2 dB can be seen in Fig. 11. The power measurements of the device in an input power range from 11 dBm to 19 dBm cannot be performed because there are no appropriate experimental instruments available, such as a pre-amplifier and an attenuator for the high linearity at this input power range.

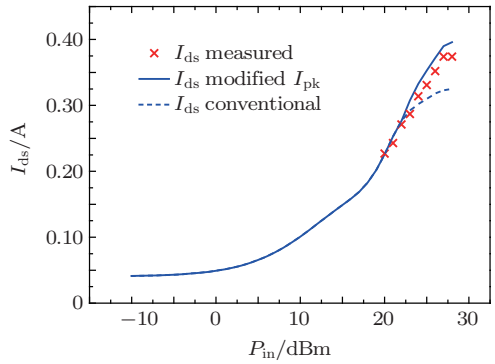


Fig. 10. (color online) Measurement (cross, only at $P_{in} = 20$ dBm–28 dBm), conventional simulation (dashed line), and improved simulation by modified I_{pk} (solid line) of drain–source current (I_{ds}) versus P_{in} at a frequency of 9.6 GHz for a device with a gate size of 10×100 μm.

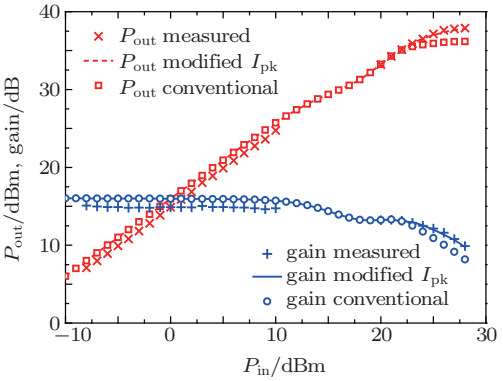


Fig. 11. (color online) Measurement (cross), conventional simulation (square), improved simulation by modified I_{pk} (dashed line) of output power and measurement (plus), conventional simulation (circle), improved simulation by modified I_{pk} (solid line) of power gain at a frequency of 9.6 GHz for a device with a gate size of 10×100 μm.

These improvements in $P_{\rm out}$ and gain are achieved from the increased maximum drain–source current ($I_{\rm max}$) of the dynamic loadline. When the modified $I_{\rm pk}$ increases, the maximum drain–source current ($I_{\rm max}$) in I–V curve also increases. As the magnitude of $P_{\rm out}$ is directly proportional to the magnitude of the maximum drain–source current ($I_{\rm max}$) as shown in Eqs. (6) and (7) from the textbook by Cripps,[17] the modified value of $I_{\rm pk}$ can directly affect the simulated $P_{\rm out}$ and gain. Figure 12 shows the effect of $I_{\rm pk}$ modification on the dynamic loadline simulation. As the value of $I_{\rm max}$ is changed due to this modification, the simulated $P_{\rm out}$ in Fig. 11 is improved.

$$I_1 = \frac{I_{\rm max}}{2\pi} \cdot \frac{\theta - \sin\theta}{1 - \cos(\theta/2)}, \tag{6}$$

$$P_{\rm out} = \frac{V_{\rm dc}}{\sqrt{2}} \cdot \frac{I_1}{\sqrt{2}}, \tag{7}$$

where I_1 is the drain–source current magnitude of fundamental frequency on the load side, $I_{\rm max}$ is the maximum amplitude of the drain–source current in the dynamic loadline, θ is the conduction angle (for class-AB, $\theta \approx \pi$–2π), and $V_{\rm dc}$ is the DC component of the drain–source voltage.

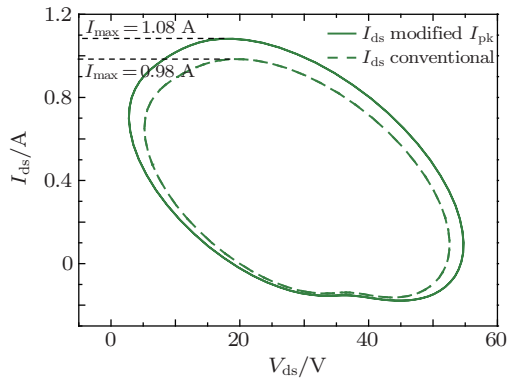


Fig. 12. (color online) Dynamic loadline simulation of AlGaN/GaN HEMT at class-AB operation point ($V_{\rm gs} = -3.5$ V, $V_{\rm ds} = 30$ V) and an operating frequency of 9.6 GHz for a device with a gate size of 10×100 μm ($P_{\rm in} = 24$ dBm).

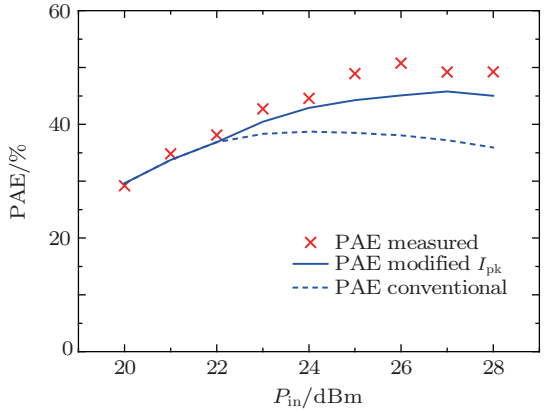


Fig. 13. (color online) Measurement (cross), conventional simulation (dashed line), and improved simulation by modified $I_{\rm pk}$ (solid line) of PAE at a frequency of 9.6 GHz for a device with a gate size of 10×100 μm.

The accuracy of PAE simulation is also improved because the accuracies of both output power and $I_{\rm ds}$ current are improved. The result of improved PAE in a high input power region is shown in Fig. 13. The highest improvement of PAE is approximately 10 per cent at an input power of 28 dBm. The improvement of simulated PAE results from more accurate simulations of drain–source current ($I_{\rm ds}$) in Fig. 10 and output power ($P_{\rm out}$) in Fig. 11, which are important factors for calculating the PAE as shown below

$$\begin{aligned} {\rm PAE}\,(\%) &= 100 \times \frac{P_{\rm out,watt} - P_{\rm in,watt}}{P_{\rm dissipated,watt}} \\ &= 100 \times \frac{P_{\rm out,watt} - P_{\rm in,watt}}{V_{\rm ds} \cdot I_{\rm ds} + V_{\rm gs} \cdot I_{\rm gs}}. \end{aligned} \tag{8}$$

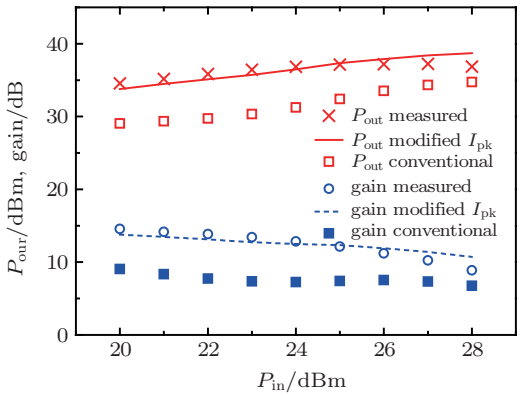


Fig. 14. (color online) Measurement (cross), conventional simulation (empty square), improved simulation by modified $I_{\rm pk}$ (solid line) of output power and measurement (circle), conventional simulation (filled square), improved simulation by modified $I_{\rm pk}$ (dashed line) of power gain at a frequency of 9.6 GHz for a device with a gate size of 8×100 μm.

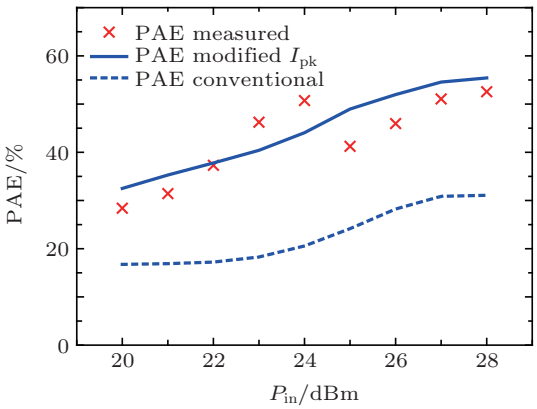


Fig. 15. (color online) Measurement (cross), conventional simulation (dashed line), and improved simulation by modified $I_{\rm pk}$ (solid line) of PAE at a frequency of 9.6 GHz for a device with a gate size of 8×100 μm.

In order to validate the proposed $I_{\rm pk}$ modification method, the steps of nonlinear model extraction in previous sections are repeated again at $V_{\rm gs} = -3.5$ V and $V_{\rm ds} = 30$ V for another device with a gate size of 8×100 μm as shown in Fig. 2(b). The power measurement via the load-pull system is performed in an input power range from 20 dBm to 28 dBm. The optimum input- and output-impedances are $10.09 + {\rm j}3.65\ \Omega$ and $35.24 + {\rm j}30.82\ \Omega$ respectively. In this case, the optimized parameters '$I_{\rm pk,DC}$', 'P_0', '$P_{\rm in,3\ dB}$', and 'β' are equal to 0.31 A, 7 dBm, 25 dBm, and 0.02 respectively. The comparisons of

output power and gain between simulation and measurement are shown in Fig. 14. The improvements of output power and gain simulations after using the modified I_{pk} are both approximately 5 dB at $P_{in} = 24$ dBm. Figure 15 shows 20% improvement in simulating PAE at $P_{in} = 24$ dBm.

6. Conclusions

The new modified drain–source current method of improving the accuracy of the model power simulation is proposed in this paper. Due to the RF dispersion effect and the nonlinearity of class-AB RF power operation of the AlGaN/GaN HEMT device, the measured drain–source current significantly increases at high input power. Since the RF drain–source current simulation has a great influence on the accuracy of the RF power simulation of the AlGaN/GaN HEMT model, the additional modification of the parameter 'I_{pk}' of the drain–source current is made for more accurately simulating the power device. The measured values and simulated values of *S*-parameters, output power, gain, and PAE at a frequency of 9.6 GHz are also presented. The results show that the simulations are highly accurate. The improvements of PAE are about 10 percent for a device with a gate size of 10×100 μm and 20 percent for a device with a gate size of 8×100 μm. The proposed method would be useful for developing the AlGaN/GaN HEMT large-signal models used in RF high power amplifier design.

Acknowledgment

The authors would like to thank Prof Dr Gao Jian-Jun from East China Normal University for his guidance, Mr Li Yan-Kui for his support for the measurement of GaN HEMT device, Dr Yao Hong-Fei and Dr Kong Xin for their fruitful discussion, and colleagues at fabrication process factory of Institute of Microelectronics, Chinese Academy of Sciences for the fabrication of the device.

References

[1] Mishra U K, Shen L, Kazior T E and Wu Y F 2008 *Proc. IEEE* **96** 287
[2] Chu F T, Chen C, Zhou W and Liu X Z 2013 *Chin. Phys. Lett.* **30** 097303
[3] Tan W S, Uren M J, Fry P W, Houston P A, Balmer R S and Martin T 2006 *Solid State Electron.* **50** 511
[4] Suebsombut P, Koch O and Chalermwisutkul S 2010 *Proceedings of IEEE Electrical Engineering/Electronics Computer Telecommunications and Information Technology Conference (ECTI-CON)*, 2010, Thailand, p. 561
[5] Ge Q, Chen X J, Luo W J, Yuan T T, Pang L and Liu X Y 2011 *J. Semicond.* **32** 085001
[6] Sheppard S T, Smith R P, Pribble W L, Ring Z, Smith T, Allen S T, Milligan J and Palmour J W 2002 *Proceedings of International Conference in the* 60th *Annual Device Research (CDR)*, 2002, University of California, Santa Barbara, USA, p. 175
[7] Monprasert G, Suebsombut P, Pongthavornkamol T and Chalermwisutkul S 2010 *Proceedings of IEEE Electrical Engineering/Electronics Computer Telecommunications and Information Technology Conference (ECTI-CON)*, 2010, Thailand, p. 566
[8] Angelov I, Zirath H and Rorsman N 1992 *IEEE Trans. Microwave Theory Tech.* **40** 2258
[9] Sang L and Schutt-Aine J E 2012 *J. Electromagnetic Waves and Application* **26** 284
[10] Liu L S, Ma J G and Ng G I 2009 *IEEE Trans. Microwave Theory Tech.* **57** 3106
[11] Ma X H, Lü M, Pang L, Jiang Y Q, Yang J Z, Chen W W and Liu XY 2014 *Chin. Phys. B* **23** 027302
[12] Zhou H, Xu Y H and Feng L 2012 *Proceedings of IEEE International Conference in Computational Problem-Solving (ICCP)*, 2012, China, p. 284
[13] Gao J 2005 *Int. J. Infrared Millim. Wave* **26** 1017
[14] Angelov I, Rorsman N, Stenarson J, Garcia M and Zirath H 1999 *IEEE Trans. Microwave Theory Tech.* **47** 2350
[15] Pu Y, Pang L, Chen X J, Yuan T T, Luo W J and Liu X Y 2011 *Chin. Phys. B* **20** 097305
[16] Gao J 2009 *RF and Microwave Modeling and Measurement Techniques for Field Effect Transistors* (Raleigh: SciTech Publishing) pp. 204–209
[17] Cripps S C 2002 *RF Power Amplifiers for Wireless Communications*, 2nd edn. (Norwood: Artech House) pp. 42–45